Transmission properties of slanted annular aperture arrays. Giant energy deviation over sub-wavelength distance

T. Alaridhee,[1] A. Ndao,[1] M.-P. Bernal,[1] E. Popov,[2] A.-L. Fehrembach[2] and F. I. Baida[1,*]

[1]*Institut FEMTO-ST, UMR 6174 CNRS, Département d'Optique P. M. Duffieux, Université de Franche–Comté, 25030 Besançon Cedex, France*

[2]*Aix-Marseille Université, CNRS, Centrale Marseille, Institut Fresnel UMR 7249, 13013 Marseille, France*

[*]*fbaida@univ-fcomte.fr*

Abstract: This paper is devoted to the study of the transmission properties of Slanted Annular Aperture Arrays made in perfectly conducting metal. More precisely, we consider the transmission based on the excitation of the cutoff-less guided mode, namely the *TEM* mode. We numerically and analytically demonstrate some intrinsic properties of the structure showing a transmission coefficient of at least 50% of an unpolarized incident beam independently of the illumination configuration (angle and plane of incidence). The central symmetry exhibited by the structure is analytically exploited to demonstrate the existence of a polarization state for which all the incident energy is transmitted through the sub-wavelength apertures when the eigenmode is excited, whatever are the illumination and the geometrical parameters. For this state of polarization, the laminar flow of the energy through the structure can exhibit giant deviation over very small distances. An example of energy flow deviation of 220^o per wavelength is presented for illustration. The results presented in this paper could be considered as an important contribution to the understanding of the enhanced transmission phenomenon based on the excitation of guided modes.

OCIS codes: (310.6628) Subwavelength structures, nanostructures; (230.7370) Waveguides; (230.0230) Optical devices; (050.1940) Diffraction; (160.3918) Metamaterials.

References and links

1. F. Aieta, P. Genevet, N. Yu, M. A. Kats, Z. Gaburro, and F. Capasso, "Out-of-plane reflection and refraction of light by anisotropic optical antenna metasurfaces with phase discontinuities," Nano Letters **12**, 1702–1706 (2012).
2. C. Genet and T. W. Ebbesen, "Light in tiny holes," Nature (London) **445**, 39–46 (2007).
3. T. W. Ebbesen, H. J. Lezec, H. F. Ghaemi, T. Thio, and P. A. Wolff, "Extraordinary optical transmission through sub-wavelength hole arrays," Nature (London) **391**, 667–669 (1998).
4. F. I. Baida, D. Van Labeke, and B. Guizal, "Enhanced confined light transmission by single subwavelength apertures in metallic films," Appl. Opt. **42**, 6811–6815 (2002).
5. J.-S. Bouillard, J. Einsle, W. Dickson, S. G. Rodrigo, S. Carretero-Palacios, L. Martin-Moreno, F. J. Garcia-Vidal, and A. V. Zayats, "Optical transmission of periodic annular apertures in metal film on high-refractive index substrate: The role of the nanopillar shape," Appl. Phys. Lett. **96**, 201101 (2010).
6. F. I. Baida, D. Van Labeke, G. Granet, A. Moreau, and A. Belkhir, "Origin of the super-enhanced light transmission through a 2-d metallic annular aperture array: a study of photonic bands," Appl. Phys. **79**, 1–8 (2004).

#234212 - $15.00 USD Received 9 Feb 2015; revised 15 Apr 2015; accepted 16 Apr 2015; published 24 Apr 2015

7. P. Banzer, J. Kindler, S. Quabis, U. Peschel, and G. Leuchs. "Extraordinary transmission through a single coaxial aperture in a thin metalfilm," Opt. Express **18**, 10896–10904 (2010).
8. X. Wang, W. Xiong, W. Sun, and Y. Zhang. "Coaxial waveguide mode reconstruction and analysis with thz digital holography," Opt. Express **20**, 7706–7715 (2012).
9. A. Moreau, G. Granet, F. I. Baida, and D. Van Labeke. "Light transmission by subwavelength square coaxial aperture arrays in metallic films," Opt. Express **11**, 1131–1136 (2003).
10. J. Salvi, M. Roussey, F. I. Baida, M.-P. Bernal, A. Mussot, T. Sylvestre, H. Maillotte, D. Van Labeke, A. Perentes, I. Utke, C. Sandu, P. Hoffmann, and B. Dwir. "Annular aperture arrays: study in the visible region of the electromagnetic spectrum," Opt. Lett. **30**, 1611–1613 (2005).
11. F. I. Baida, A. Belkhir, D. Van Labeke, and O. Lamrous. "Subwavelength metallic coaxial waveguides in the optical range: Role of the plasmonic modes," Phys. Rev. B **74**, 205419 (2006).
12. F. I. Baida. "Enhanced transmission through subwavelength metallic coaxial apertures by excitation of the tem mode," Appl. Phys. B **89**, 145–149 (2007).
13. F. I. Baida, A. Belkhir, O. Arar, E. Barakat, J. Dahdah, C. Chemrouk, D. Van Labeke, C. Diebold, N. Perry, and M.-P. Bernal. "Enhanced optical transmission by light coaxing: Mechanism of the tem-mode ," Micron **41**, 742–745 (2010).
14. A. Roberts. "Beam transmission through hole arrays," Opt. Express **18**, 2528–2533 (2010).
15. M. Hamidi, C. Chemrouk, A. Belkhir, Z. Kebci, A. Ndao, O. Lamrous, and F. I. Baida. "SFM-FDTD analysis of triangular-lattice AAA structure: Parametric study of the TEM mode," Opt. Commun. **318**, 47–52 (2014).
16. A. Ndao, A. Belkhir, R. Salut, and F. I. Baida. "Slanted annular aperture arrays as enhanced-transmission metamaterials: Excitation of the plasmonic transverse electromagnetic guided mode," Appl. Phys. Lett. **103**, 211901 (2013).
17. R. de Waele, S. P. Burgos, A. Polman, and H. A. Atwater. "Plasmon dispersion in coaxial waveguides from single-cavity optical transmission measurements," Nano Letters **9**, 2832–2837 (2009).
18. R. Fan, M. Yue, R. Karnik, A. Majumdar, and P. Yang. "Polarity switching and transient responses in single nanotube nanofluidic transistors," Phys. Rev. Lett. **95**, 086607 (2005).
19. Y. Poujet, J. Salvi, and F. I. Baida. "90% extraordinary optical transmission in the visible range through annular aperture metallic arrays," Opt. Lett. **32**, 2942–2944 (2007).
20. D. Van Labeke, D. Gérard, B. Guizal, F. I. Baida, and L. Li. "An angle-independent frequency selective surface in the optical range," Opt. Express **14**, 11945–11951 (2006).
21. E. Barakat, M.-P. Bernal, and F. I. Baida. "Doubly resonant Ag-$LiNbO_3$ embedded coaxial nanostructure for high second-order nonlinear conversion," J. Opt. Soc. Am. B **30**, 1975–1980 (2013).
22. A. Belkhir and F. I. Baida. "Three-dimensional finite-difference time-domain algorithm for oblique incidence with adaptation of perfectly matched layers and nonuniform meshing: Application to the study of a radar dome," Phys. Rev. E **77**, 056701 (2008).
23. E. Barakat, M.-P. Bernal, and F. I. Baida. "Theoretical analysis of enhanced nonlinear conversion from metallo-dielectric nano-structures," Opt. Express **20**, 16258–16268 (2012).
24. A. A. E. Saleh and J. A. Dionne. "Toward efficient optical trapping of sub-10-nm particles with coaxial plasmonic apertures," Nano Letters **12**, 5581–5586 (2012).
25. J. Dahdah, J. Hoblos, and F. I. Baida. "Nanocoaxial waveguide grating as quarter-wave plates in the visible range," IEEE Photon. J. **4**, 87–94 (2012).
26. A.-L. Fehrembach, D. Maystre, and A. Sentenac. "Phenomenological theory of filtering by resonant dielectric gratings," J. Opt. Soc. Am. A **19**, 1136–1144 (2002).
27. E. Popov, L. Mashev, and D. Maystre. "Theoretical study of the anomalies of coated dielectric gratings," Opt. Acta **33**, 607–619 (1986).
28. A.-L. Fehrembach and A. Sentenac. "Study of waveguide grating eigenmodes for unpolarized filtering applications," J. Opt. Soc. Am. A **20**, 481–488 (2003).
29. A.-L. Fehrembach, K. Chan Shin Yu, A. Monmayrant, P. Arguel, A. Sentenac, and O. Gauthier-Lafaye. "Tunable, polarization independent, narrow-band filtering with one-dimensional crossed resonant gratings," Opt. Lett. **36**, 1662–1664 (2011).

1. Introduction

The enhanced light transmission (ET) phenomenon through sub-wavelength apertures in metal plates have already attracted researchers' attention [1, 2]. This is mainly due to the observation made by T. W. Ebbesen's team of an extraordinary optical transmission (EOT) which inevitably revolutionized the field of nano-optics and opened a wide range of applications from spectral filtering to nano-antennas via single molecule spectroscopy [3]. Plasmonics has taken full advantage of this boom because the high transmission was associated with the excitation of a surface plasmon resonance of the metallic layer that supports the engraved sub-wavelength

#234212 - $15.00 USD Received 9 Feb 2015; revised 15 Apr 2015; accepted 16 Apr 2015; published 24 Apr 2015

apertures [4, 5]. Nonetheless, enhanced transmission could be obtained through a simple phenomenon of light guiding in even smaller apertures without the need of plasmons [6–8]. In fact, some metallic waveguide geometries (section shape) allow the existence of a guided mode with a relatively large cutoff wavelength compared to the waveguide transverse dimensions. This is specially the case of waveguides having a multi-connected conductor contours such as the coaxial waveguide (bi-connected) [9–11]. Indeed, the fundamental mode of such waveguide is a Transverse ElectroMagnetic (TEM) mode that has no cutoff [12]. Enhanced transmission through annular aperture arrays (AAA) due to the excitation of this peculiar mode was already theoretically studied [13–15] and recently experimentally demonstrated [16]. However, very difficult experimental constraints (especially the implementation of a large angle of incidence) must be met in order to obtain efficient excitation of the TEM mode [17]. More than ten years ago, efficient enhanced transmission (up to 93% in the visible range) through these AAAs was obtained using the excitation of the second guided mode [18, 19], the TE_{11} mode that exhibits a large wavelength cutoff compared to the waveguide diameter. The properties of the EOT based on the excitation of this mode were studied by several groups. For example, it was clearly demonstrated that the resulting ET is angle and polarization independent [20] since the diffraction anomalies (Wood and Rayleigh) are spectrally far from the transmission peak position. In addition, due to the small metal thickness, the TE_{11} mode is mainly excited at its cutoff, meaning that it is associated to a very low group velocity and a quasi-infinite phase velocity [21]. All these attributes provide quite interesting properties for applications in various fields as the protection of radars (radomes) [22], photovoltaic, non-linear enhancement [23], optical trapping [24] or also in the design of metamaterials with giant artificial birefringence [25].

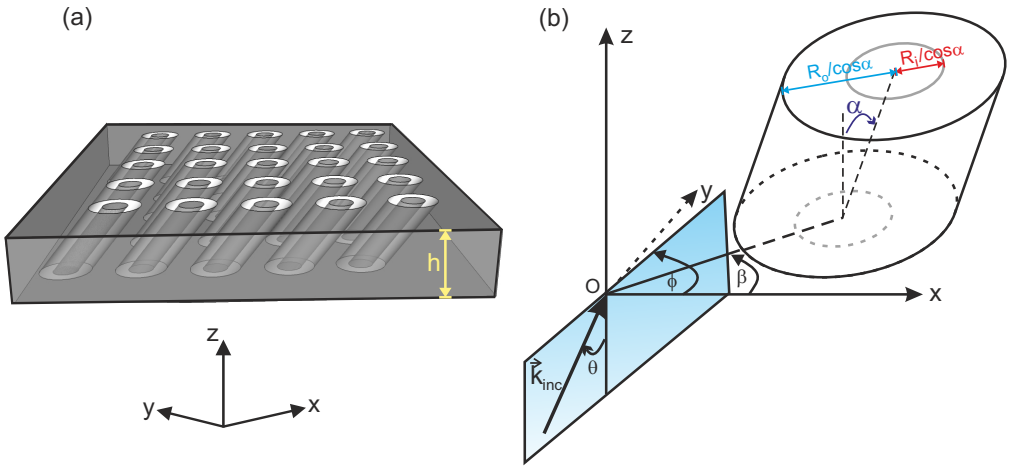

Fig. 1. (a) 3D view of the Slanted Annular Aperture Array (SAAA) structure under consideration. (b) Schema showing the different geometrical parameters used to assign the incident wave-vector position (in the plane formed by the Oz axis at an angle ϕ from the Ox axis) and direction (incidence angle θ counted from the Oz axis). The aperture axis is tilted by an angle α from the vertical direction (Oz) in a plane also located at an angle β from the Ox axis). The horizontal section of on aperture has then outer (inner) ellipses with minor half axis R_o (R_i) and major $R_o/\cos\alpha$ ($R_i/\cos\alpha$).

2. The SAAA structure

Recently, in order to bypass the experimental constraints associated with the excitation of the TEM mode, a slanted annular aperture array (SAAA) structure (see Fig. 1) was proposed,

#234212 - $15.00 USD Received 9 Feb 2015; revised 15 Apr 2015; accepted 16 Apr 2015; published 24 Apr 2015

fabricated and characterized [16]. Indeed, the TEM mode is then excited at normal incidence and its spectral position is red-shifted compared to the conventional AAA structure. In fact, due to the inclined path through the metal film, the effective thickness of the cavities is larger and the phase matching condition can be fulfilled for larger values of the wavelength. Unfortunately, the TEM-based transmission in the visible range was weak due to metal losses and to the fact that this TEM-like mode is spatially extended in the metal more than the TE_{11} mode. Thus, in this paper, we will address theoretical and numerical simulations (through homemade 3D-Finite Difference Time Domain algorithm) only in case of microwave and THz domain where metals can be considered as perfectly electric conductors leading to efficient transmission as shown in Fig. 2. In this figure, a comparison between the transmission of an AAA and a SAAA structures (see Fig. 2(a)) having the same film thickness (h) is presented. The AAA structure is illuminated at oblique incidence with an angle of incidence equals to the tilt angle ($\theta = \alpha$) of the SAAA structure while this later is illuminated at normal incidence. The incident polarization is TM (magnetic field perpendicular to the plane of incidence); As shown in Fig. 2(b) the TEM-based transmission peak appears and reaches 100% for both structures. Nevertheless, its spectral position is significantly redshifted when the apertures are tilted. Indeed, since the Rayleigh anomaly is far from the spectral position λ_{TEM} of the TEM-based transmission peak (structure period $p < \pi(R_i + R_o)$), λ_{TEM} can be given by a phase matching relation:

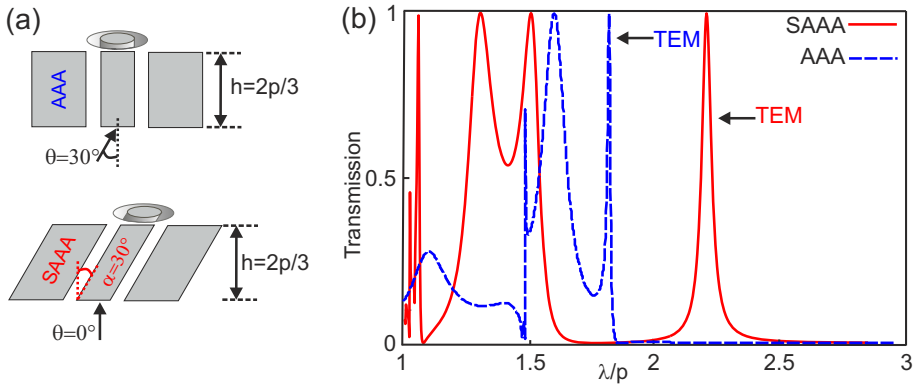

Fig. 2. Calculated transmission spectra for two different configurations (a) having the same metal thickness $h = 2p/3$ where p is the period along Ox and Oy directions. (b) The red curve represents the transmission through the SAAA structure at normal incidence while the blue one corresponds to the transmission through the AAA structure. For both structures, we consider a TM polarized incident plane wave with $\phi = \beta = 0^o$ (see Fig. 1) but $\theta = 0^o$ and $\alpha = 30^o$ for the SAAA structure and $\theta = 30^o$ in the case of the AAA structure. For the two configurations, we fixed the radii values to $R_o = p/3$ and $R_i = p/6$.

$$\lambda_{TEM} = \frac{4\pi n_{eff} h_{eff}}{(2m\pi - \phi_r)} \quad \text{with } \{h_{eff} = h \text{ for AAA}\} \text{ and } \{h_{eff} = h/\cos(\alpha) \text{ for SAAA}\} \quad (1)$$

where m is a non-zero positive integer, n_{eff} is the real part of the effective index of the TEM mode ($n_{eff} = 1$ if perfect conductor) and ϕ_r is a phase change due to the mode reflection (and diffraction) at the input or the output side. α is the angle of the aperture tilt counted from the normal to the metal interface. The position of the TEM peak can then be tuned through the tilt angle for a fixed value of the thickness. Nevertheless, this dependence is not completely explicit because the phase term (ϕ_r) can also depend on α. In order to gain more insight, we have studied the transmission response as a function of α at a fixed value of the thickness

#234212 - $15.00 USD Received 9 Feb 2015; revised 15 Apr 2015; accepted 16 Apr 2015; published 24 Apr 2015

$h = 2p/3$ and in the case of normal incidence. In both cases, the radii of the annular aperture are fixed to $R_o = p/3$ and $R_i = p/6$. The results are plotted in Fig. 3(a) for α varying from 5^o to 45^o. As expected from Eq. (1), the TEM peak position shifts to the red region of the spectrum when α increases ($1/\cos\alpha$ increases). Figure 3(b) depicts the spectral positions of the TEM peak as a function of $1/\cos\alpha$ (solid blue curve). An almost linear behavior is obtained meaning that the phase ϕ_r is quite constant when α varies. The slight discrepancy appearing at small values of α between the numerical calculation and that obtained from Eq. (1) when considering $\phi_r = 1.9$ rad (dashed red line) is attributed to the coupling between the TEM and the TE_{11} modes. Thus, the light is totally transmitted through the structure independently of the value of α but at different wavelengths.

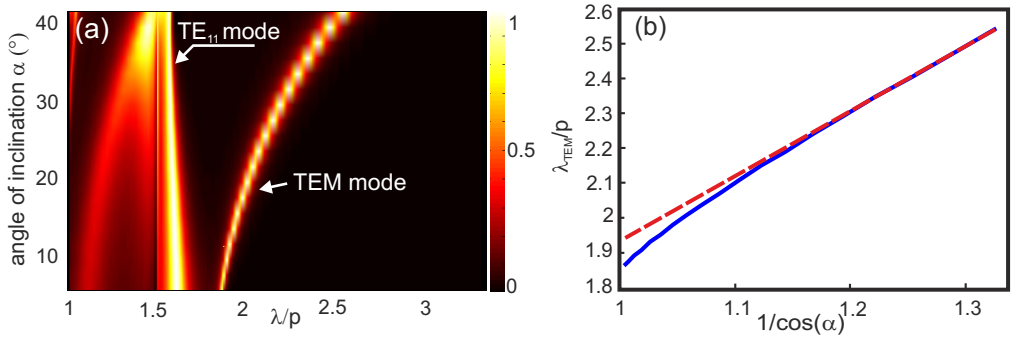

Fig. 3. (a) Transmission spectra in color level versus the tilt angle α of a SAAA with metal thickness $h = 2p/3$ (p is the period of the grating along the Ox and Oy directions), the inner and outer radii of the coaxial cavities are $R_i = p/6$ and $R_o = p/3$ respectively. The structure is illuminated by a TM polarized plane wave at normal incidence with $\phi = \beta = 0^o$. (b) The solid blue curve is the spectral position of the TEM-based transmission peak function of $1/\cos(\alpha)$. The dashed red curve corresponds to the asymptotic linear behavior when we consider ϕ_r constant.

On the other hand, Eq. (1) does not show any explicit relation between λ_{TEM} and the angle of incidence θ. Nonetheless, one can intuitively suspect a relation between this angle and the phase term ϕ_r. Numerical simulations presented in Fig. 4(a), corresponding to a tilt angle $\alpha = 35^o$ and an angle of incidence that varies from -45^o to 45^o, show that the spectral position and the maximum value (100%) of the TEM-based transmission peak is independent of the angle of incidence. Only the quality factor (peak sharpness) is affected and it is maximum at normal incidence. In addition, for the sub-wavelength regime, there is a perfect symmetry of the transmission variations with respect to the normal incidence ($T(-\theta) = T(\theta)$), as shown in Fig. 4(b), where two spectra corresponding to $\theta = \pm 40^o$ are plotted. This property is a consequence of the energy balance and the reciprocity theorem as analytically demonstrated in the appendix (see paragraphs 1 and 3) from the study of the transmission scattering matrix [26, 27]. The symmetry of the spectra with respect to the angle of incidence can be understood intuitively by the fact that the apertures are sub-wavelength details of the structure, and therefore cannot be detected in the far-field. On the contrary, for $\lambda < \lambda_{Rayleigh}$ the transmission spectra do not exhibit any symmetry. In this spectral range, propagating diffracted orders exist and their efficiencies depend on the tilt angle. Consequently, the diffracted zero order transmission changes with respect to the energy carried by these homogeneous orders. The obtained symmetry breaking, due to energy loss in the propagated diffraction orders, is clearly illustrated in Fig. 4(b) where the diffracted zero order is more efficient when the angle between the incident light and the aperture axis (tilt direction) is small (blue curve of Fig. 4(b)) compared to the opposite incident

#234212 - $15.00 USD Received 9 Feb 2015; revised 15 Apr 2015; accepted 16 Apr 2015; published 24 Apr 2015

angle case (red curve of Fig. 4(b)). Let us notice that the property of symmetry with respect to the angle of incidence is valid for any resonance of the transmission as illustrated in the same Fig. 4(a) where the two TE_{11}-based transmission peaks exhibit the same symmetry properties with respect to the normal incident axis ($\theta = 0^o$) and also reach 100% independently of the angle of incidence. Nevertheless, for large values of θ (20^o), the Rayleigh anomaly approaches the TE_{11}-based transmission peaks and a coupling between the two resonances occur resulting in a modification of the transmission properties.

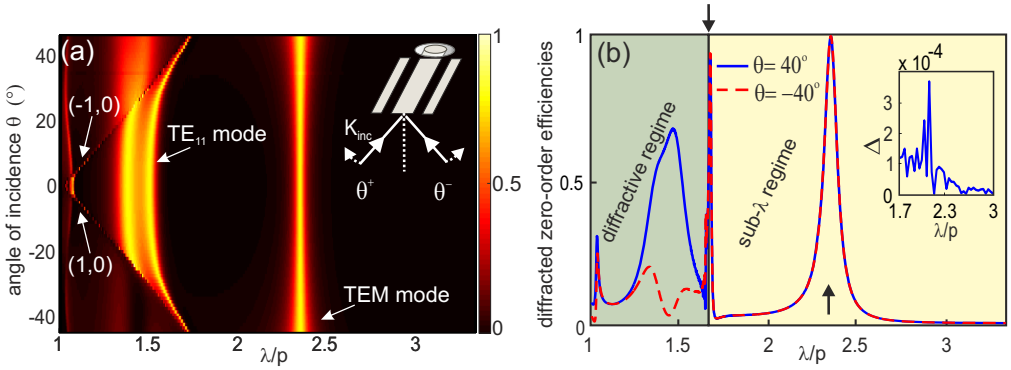

Fig. 4. (a) Calculated transmission spectra in color level versus the angle of incidence. Inset of (a) presents the illumination direction with respect to the tilt angle. Two Rayleigh anomalies can be seen in the figure and are indicated by the value of the (m,l) corresponding to diffracted order (m along x and l along y axis). (b) two cross-sections made on (a) and illustrating the transmission spectra for two angles of incidence $\theta = 40^o$ in solid blue line and $\theta = -40^o$ in dashed red line. Note that the up- and down-arrows indicate the position of TEM-based transmission peak and the Rayleigh anomaly respectively whereas the value of the tilt angle is fixed to $\alpha = 35^o$. The inset of (b) shows the residual numerical signal ($\Delta = |T(\theta = 40^o) - T(\theta = -40^o)|$) corresponding to the difference between the two spectra only in the sub$-\lambda$ range.

3. Transmission properties

As already mentioned, an important information from these spectra is that, for the SAAA structure, which exhibits a central symmetry (see Appendix), the transmission reaches 100% at the wavelength resonance whatever the angle of incidence for a fixed value of the tilt angle. This property is replaced with another surprising property when one considers planes of incidence that are not along a direction of periodicity of the structure, as shown in Fig. 5, where different illumination configurations are considered by varying both the angle of incidence θ and the azimuthal one ϕ assuming $\beta = 0^o$. For each couple (θ, ϕ), the two polarization states (TE, TM) are studied and we found that the sum of the transmission at the TEM-based peak is equal to 100% whatever the couple (θ, ϕ) is. In Figs. 5(a,b) and 5(e,f), we also observe the discontinuities corresponding to Rayleigh anomalies indicated by the indexes ((0,-1) and (-1,0)). The fact that for the structure under study, the sum of the transmittivities for TE and TM incident polarizations is equal to 100% at resonance whatever the angle of incidence, can be explained by analyzing the eigenvectors and eigenvalues of the $T_1^* T_1$ matrix, where T_1 is the scattering matrix of the structure and T_1^* is the conjugate transpose of T_1. The details are presented in the Appendix, which extends the demonstrations made in [26] and [27]. To sum-up, the two eigenvalues of the $T_1^* T_1$ matrix are real and positive and they are the limits of the range of variation of the transmittivity when the polarization of the incident plane wave takes all possible states,

#234212 - $15.00 USD Received 9 Feb 2015; revised 15 Apr 2015; accepted 16 Apr 2015; published 24 Apr 2015

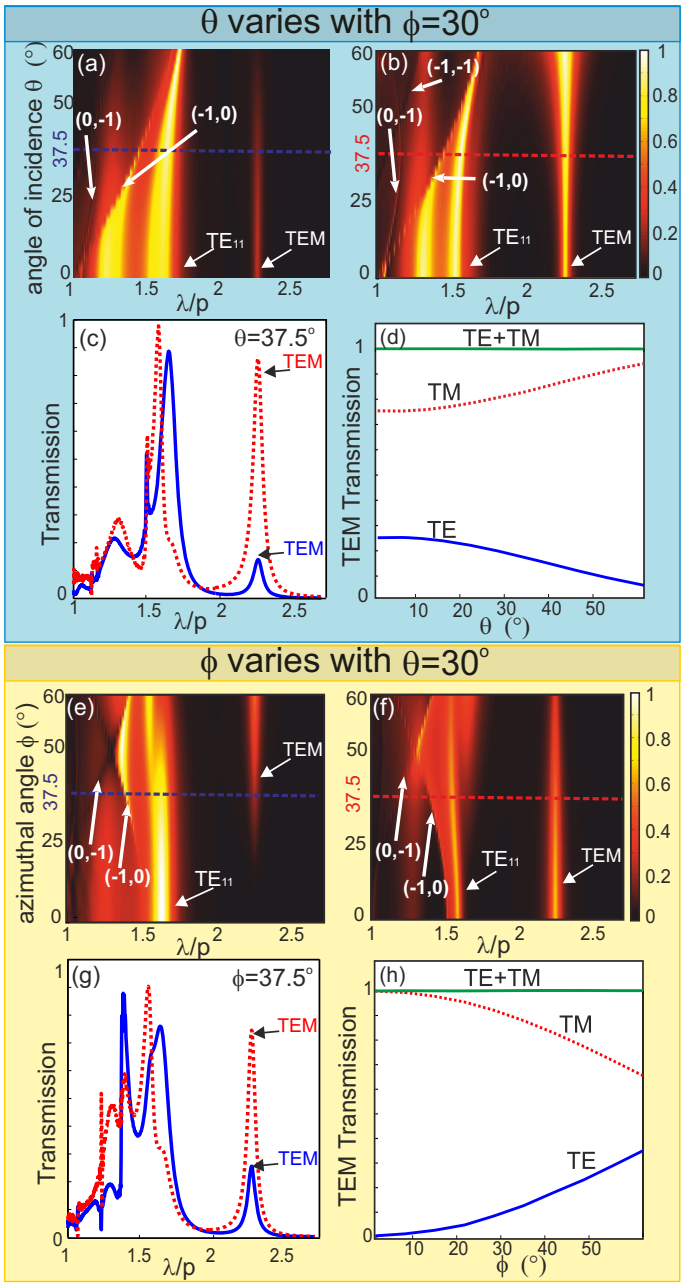

Fig. 5. (Top) Transmission spectra for different angles of incidence in both TE (a) and TM (b) polarizations obtained for an arbitrary azimuthal angle $\phi = 30^o$. (c) Cross-sections made over (a) and (b) at $\theta = 37.5^o$. (d) Transmission efficiencies at λ_{TEM} of the two polarization states (TM in dashed red line and TE in solid blue line) and their sum (green horizontal line) as a function of the angle of incidence θ. (Bottom) Transmission spectra for different azimuthal angles ϕ values in both TM (e) and TE (f) polarizations for an angle of incidence of $\theta = 30^o$. (g) Cross-sections made over (e) and (f) at $\phi = 37.5^o$. (h) Transmission efficiencies at λ_{TEM} of the two polarization states (TM in dashed red line and TE in solid blue line) and their sum (green horizontal line) as a function of the azimuthal angle ϕ.

#234212 - $15.00 USD Received 9 Feb 2015; revised 15 Apr 2015; accepted 16 Apr 2015; published 24 Apr 2015

even non linear polarization states (see the Appendix, first paragraph). The only necessary assumption is that the only propagative diffraction order is the zero order. The two eigenvectors, which are orthogonal to each other, correspond to the polarizations of the incident wave that allow to obtain these limits of transmittivity. Hence, it appears that it is better to work with the eigenvalues and eigenvectors of the $T_1^* T_1$ matrix rather than with the transmittivities for TE and TM incident polarizations, especially for structures leading to polarization conversion.

Furthermore, if the structure has a symmetry center (see Fig. 6), it is possible to show (see the Appendix, paragraph 2-4) that one eigenvalue of the $T_1^* T_1$ matrix reaches 100% when one eigenmode is excited, provided that the materials are lossless. Note that if the structure is symmetrical with respect to an axis normal to the plane containing the directions of periodicity of the structure, the same property occurs for the reflectivity, while if the structure is symmetrical with respect to a plane containing the directions of periodicity, both reflectivity and transmittivity reaches 100% for neighbouring wavelengths around resonance, as shown in [26] and [27].

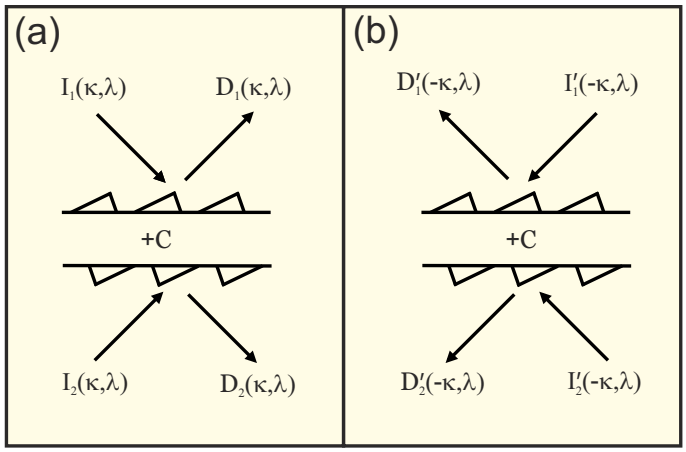

Fig. 6. General scheme of a structure exhibiting a central symmetry in (a) and the reciprocal configuration in (b).

Coming back to the SAAA structure presenting a center of symmetry, we can say that there exists a polarization state (P_{max}) for which the transmission reaches 100%. Moreover, in our case, as we consider small apertures in a metallic plate, the orthogonal P_{min} polarization state leads to a negligible transmission, or eventually to a residual transmission due, for example, to the presence of another resonance at a different wavelength. The P_{max} polarization is clearly the TM polarization when $\beta = \phi = 0$ (see Fig. 7), meaning a plane of incidence parallel to the aperture axis. In the general case of arbitrary incident polarization, because of the fact that the P_{max} and P_{min} polarization are orthogonal to each other, the sum of the transmittivities for TE and TM polarizations is equal to the sum of the eigenvalues of the $T_1^* T_1$ matrix, hence is close to 100%. This property is numerically verified through the results presented in Fig. 5 where different illumination configurations are considered by varying both the angle of incidence θ and the azimuthal one ϕ assuming $\beta = 0^o$. For each couple (θ, ϕ), the two polarization states (TE, TM) are studied and we found that the sum of the transmission at the TEM-based peak is equal to 100% whatever the couple (θ, ϕ) is.

Let us now consider an arbitrary configuration where ϕ and β are simultaneously nonzero and different from each other. Consequently, we have fixed the geometrical and illumination parameters to : $R_i = p/6, R_o = p/3, h = 2p/3, \alpha = 30^o, \phi = 65^o, \beta = 25^o$ and $\theta = -35^o$. Figure 7(a) presents the numerical transmission spectra where the dashed red line and the solid blue

#234212 - $15.00 USD Received 9 Feb 2015; revised 15 Apr 2015; accepted 16 Apr 2015; published 24 Apr 2015

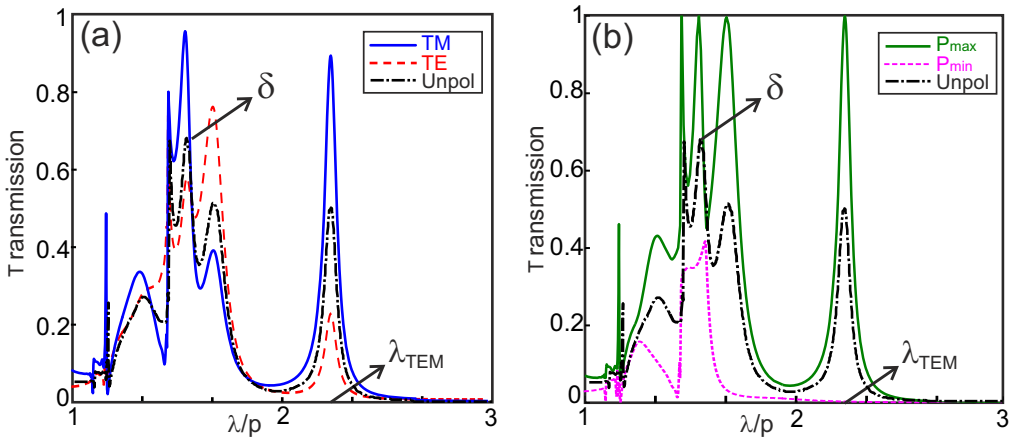

Fig. 7. Transmission spectra of an arbitrary SAAA structure where $\beta = 25^o, R_o = p/3, R_i = p/6, h = 2p/3$ illuminated by a linearly polarized plane wave with $\phi = 65^o$ and $\theta = -35^o$. (a) The solid blue line corresponds to the case of a TM polarization while the dashed red one fits the case of a TE polarization. The dotted black line presents the transmission of an unpolarized incident beam. (b) Transmission spectra for the two polarization states (P_{max}, P_{min} that correspond to the two eigenvalues of the matrix $T_1^* T_1$). Note that the polarization states P_{max} and P_{min} vary with the wavelength. The dotted black line is the same as in (a) because it equals to $(P_{max} + P_{min})/2 = (TE + TM)/2$.

one correspond to the TE and TM polarization states respectively. Once again, the sum of the transmission at λ_{TEM} is equal to 1. The two eigenvalues of the $T_1^* T_1$ matrix are plotted in Fig. 7(b) where the solid green line corresponds to the polarization state P_{max} while the dashed magenta one represents the P_{min} state. As expected, perfect transmission is obtained at λ_{TEM} for the P_{max} polarization while an almost zero transmission (2.6% only) occurs for the orthogonal polarization P_{min}. Note that, for the P_{max} polarization, other transmission maxima (up to 100%) arise corresponding to additional transmission resonances (especially due to the excitation of the TE_{11} guided mode at two different wavelength values corresponding to Fabry-Perot harmonics). It is important to note that the eigenvectors corresponding to the eigenvalues plotted in Fig. 7(b) generally vary with the wavelength, hence, the polarization state allowing a 100% transmittivity may not be the same when the TEM and the TE_{11} modes are excited. From this study, it appears that when one eigenmode is excited, the transmission efficiency of an unpolarized incident beam at the resonance wavelength is, at least, equal to 50%. This is confirmed by the plot of the transmittivity for an unpolarized wave in Fig. 7 Another conclusion is that a necessary condition to obtain a polarization independent transmittivity at resonance is to excite two eigenmodes.

4. Giant energy deviation

Finally, let us emphasize that in the sub-wavelength regime, at λ_{TEM} and for the polarization state P_{max}, the incident energy is totally routed through the apertures for every value of the tilt angle. As an example, we consider a SAAA structure with $\alpha = 35^o$ illuminated by a plane wave propagating at $\theta = \pm 75^o$. The calculated transmission spectra for the P_{max} polarization state are presented in Fig. 8(a). A TEM-based transmission peak occurs at $\lambda_{TEM} = 2.3p$ whatever the sign of θ. In order to visualize the energy propagation in the vicinity of the SAAA, the energy flow (Poynting vector) is also calculated and presented in a vertical plane containing the axis of the apertures. One can clearly see in Figs. 8(b) and 8(c) the giant bending of light that occurs

#234212 - $15.00 USD Received 9 Feb 2015; revised 15 Apr 2015; accepted 16 Apr 2015; published 24 Apr 2015

over a distance as small as $\lambda/5$ (see the direction change of the white arrows at the bottom of the structure). In the vicinity of the structure, the light energy follows a serpentine path with laminar flow (total transmission) through the nano-structured metallic film after suffering a total deviation of 220^o over a distance smaller than the wavelength.

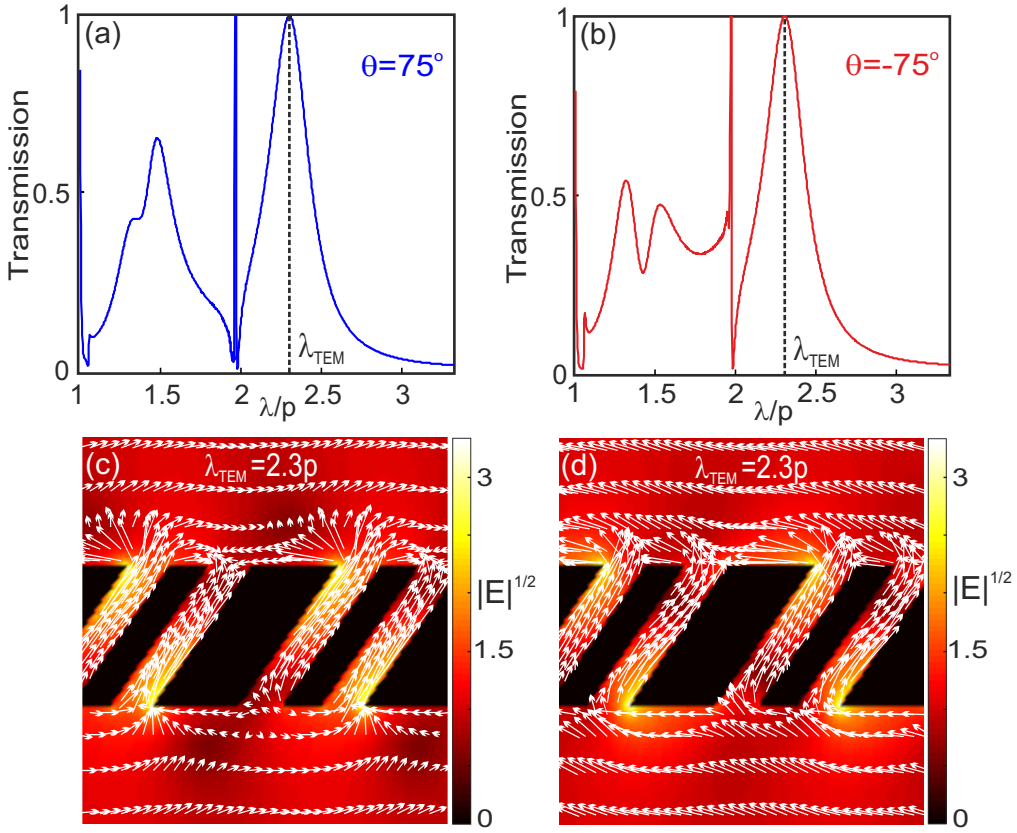

Fig. 8. Transmission spectra for an angle of incidence $\theta = 75^o$ in (a) and $\theta = -75^o$ in (b) for the same SAAA structure of Fig. 2. (c) Square root of the electric field amplitude distributions (in color map) around the nano-structured metallic film in a vertical plane containing the aperture axis for an illumination at $\theta = 75^o$. White arrows correspond the the tangential Poynting vector. (d) Same as (c) for $\theta = -75^o$.

5. Conclusion

In summary, we have studied the fundamental aspect of the enhanced transmission mechanism through the SAAA structure on the basis of both numerical and analytical calculations. As an additional result, we presented some properties of this structure that demonstrate a high potential for applications in various fields such as spectral filtering regardless of the illumination direction. The next step should address the potential enhancement of the transmission of unpolarized beams (more than 50%) by spectrally approaching two different resonances (here the TEM and the TE_{11} ones) without causing destructive coupling through a degeneracy breaking. This may require an acurate optimization of the parameters of the structure or more complex structures, as it was done in the case of all dielectric sub-wavelength periodic structures presenting a resonance peak due to the excitation of a leaky guided mode (guided mode resonance

#234212 - $15.00 USD Received 9 Feb 2015; revised 15 Apr 2015; accepted 16 Apr 2015; published 24 Apr 2015

grating) [28, 29] . Nevertheless, the case of larger transmission of about 70% can be found in Fig. 7(b) and corresponds to a transmission based on the excitation of the TE_{11} mode (see peak δ in Fig. 7). The discussion of this result is very simple but it is out of the paper scope. The giant deviation of the energy flux over small distance presented in Figs. 8(c) and (d), brings a supplementary and comprehensive physical insight about the guided mode-based enhanced transmission paradigm without the need to resort to surface plasmons or other surface waves.

Appendix

We consider a periodic structure composed of lossless materials which presents only one propagating diffraction order (the zero order). From the study of the scattering matrix of the structure, we will derive some properties of its transmittivity. This appendix is an extension of the works published in [27] and [26], and similar properties could be derived for the reflectivity.

In the following, we will first show that the eigenvalues of the transmittivity matrix for the energy, denoted $\mathbf{T_1^* T_1}$ hereafter, are the limits of the variation of the transmittivity when the incident polarization takes all possible states, and that they are obtained for orthogonal polarizations (given by the eigenvectors). Thus, these eigenvalues are the key variables to understand the behavior of a sub-wavelength grating with respect to the incident polarization. This is true especially in the case where the eigenvectors are not simply the *s* and *p* vectors, which occurs in conical incidence or when particular eigenmodes are excited.

Second, using only the reciprocity theorem and the energy balance, and with no hypothesis on the symmetry of the structure, we will show that the eigenvalues of $\mathbf{T_1^* T_1}$ are unchanged when the angle of incidence is changed in its opposite, hence generalizing a property that is well know for gratings illuminated in classical incidence (plane of incidence perpendicular to the grating grooves). This is a new result that was not published in [26].

Third, we consider structures having a central symmetry (examples are shown in Figs. 1 and 6). This kind of symmetry was discussed in [27] which focused on gratings illuminated under classical incidence (plane of incidence containing a direction of periodicity) for which there is no polarization conversion, but it was not discussed in [26]. We show that when one mode is excited, one eigenvalue of $\mathbf{T_1^* T_1}$ reaches 100% at resonance. This means that the transmittivity is equal to 100% at the resonance wavelength when the incident polarization corresponds to that of the eigenvector associated with this eigenvalue, while the transmittivity is equal to the transmittivity of the structure out of resonance for the orthogonal polarization.

.1. *From the scattering matrix to the transmittivity*

We start from the scattering matrix $\mathbf{S}(\kappa,\lambda)$ relating the incoming field (from the substrate and the superstrate), with wavelength λ and wave-vector with in-plane component κ (lying in the xy-plane in Fig. 6), to the field diffracted by the structure in the zero order of diffraction. The reader can refer to [26] (sections 2 and 3) for a full definition of the scattering matrix and of the *s* and *p* vectors associated to each incident and diffracted field (in the superstrate and the substrate). This 4x4 matrix is composed with 4 blocks:

$$\mathbf{S}(\kappa,\lambda) = \begin{pmatrix} \mathbf{R_1}(\kappa,\lambda) & \mathbf{T_2}(\kappa,\lambda) \\ \mathbf{T_1}(\kappa,\lambda) & \mathbf{R_2}(\kappa,\lambda) \end{pmatrix}. \tag{2}$$

The reflection and transmission matrices $\mathbf{R_j}$ and $\mathbf{T_j}$, where the subscript $j = 1$ (resp. $j = 2$) is used when the incident field comes from the superstrate (resp. substrate), are 2x2 matrix. They contain the reflection and transmission conversion coefficients of a *s* or *p* polarized field to a *s* or *p* polarized field. For example, $\mathbf{T_1}$ writes as

#234212 - $15.00 USD Received 9 Feb 2015; revised 15 Apr 2015; accepted 16 Apr 2015; published 24 Apr 2015

$$\mathbf{T_1} = \begin{pmatrix} t_1^{ss} & t_1^{sp} \\ t_1^{ps} & t_1^{pp} \end{pmatrix}. \tag{3}$$

From the definition of the scattering matrix it follows that the energy τ transmitted in the substrate when the incident field comes from the superstrate only can be written as:

$$\tau = l_a^{T_1^* T_1} \left| \left\langle \mathbf{I_1} | \mathbf{V_a^{T_1^* T_1}} \right\rangle \right|^2 + l_b^{T_1^* T_1} \left| \left\langle \mathbf{I_1} | \mathbf{V_b^{T_1^* T_1}} \right\rangle \right|^2, \tag{4}$$

where $l_a^{T_1^* T_1}$ and $l_b^{T_1^* T_1}$, are the eigenvalues and $\mathbf{V_a^{T_1^* T_1}}$ and $\mathbf{V_b^{T_1^* T_1}}$ the eigenvectors of the matrix $\mathbf{T_1^* T_1}$, and $\mathbf{I_1}$ is a two-elements vector containing the *s* and *p* components of the amplitude of the incident field vector.

It is important to note that $\mathbf{T_1^* T_1}$ is a hermitian matrix, thus its eigenvectors are orthogonal (in the sense of hermitian scalar product) to each other and its eigenvalues are real and positive. Hence, from Eq. (4), it follows that $l_a^{T_1^* T_1}$ and $l_b^{T_1^* T_1}$ are the limits of the variation of the transmittivity when the incident field takes all possible states of polarization (even non linear). These limits are obtained for two orthogonal polarizations. Moreover, for any two incident orthogonal polarizations, the sum of the transmittivity is equal to the sum of the eigenvalues.

.2. *Properties of the scattering matrix*

Several properties of the scattering matrix can be deduced from the energy balance and the reciprocity theorem. Again, the demonstration is given in [26] (section 3 and 5), and only the results will be reported here. Note that in the following, we will need to consider the scattering matrix for complex wavelengths. Hence, we use an expression of the energy balance suitable for a complex variable λ with complex conjugate $\overline{\lambda}$:

$$\mathbf{R_1}^*(\kappa,\overline{\lambda})\mathbf{R_1}(\kappa,\lambda) + \mathbf{T_1}^*(\kappa,\overline{\lambda})\mathbf{T_1}(\kappa,\lambda) = \mathbf{1} \tag{5}$$

$$\mathbf{R_2}^*(\kappa,\overline{\lambda})\mathbf{R_2}(\kappa,\lambda) + \mathbf{T_2}^*(\kappa,\overline{\lambda})\mathbf{T_2}(\kappa,\lambda) = \mathbf{1} \tag{6}$$

$$\mathbf{R_1}^*(\kappa,\overline{\lambda})\mathbf{T_2}(\kappa,\lambda) + \mathbf{T_1}^*(\kappa,\overline{\lambda})\mathbf{R_2}(\kappa,\lambda) = \mathbf{0} \tag{7}$$

$$\mathbf{T_2}^*(\kappa,\overline{\lambda})\mathbf{R_1}(\kappa,\lambda) + \mathbf{R_2}^*(\kappa,\overline{\lambda})\mathbf{T_1}(\kappa,\lambda) = \mathbf{0} \tag{8}$$

where **1** stands for the unit diagonal matrix of size 2x2.

The reciprocity theorem entails that $\mathbf{S}(-\kappa,\lambda) = t(\mathbf{S}(\kappa,\lambda))$ (where $t(\mathbf{S})$ is the transpose of **S**) which can be written as:

$$\mathbf{R_1}(-\kappa,\lambda) = t(\mathbf{R_1}(\kappa,\lambda)) \tag{9}$$

$$\mathbf{R_2}(-\kappa,\lambda) = t(\mathbf{R_2}(\kappa,\lambda)) \tag{10}$$

$$\mathbf{T_2}(-\kappa,\lambda) = t(\mathbf{T_1}(\kappa,\lambda)). \tag{11}$$

Now, we shall demonstrate a property related to the symmetry of the structure with respect to a symmetry center C. We consider two configurations, as depicted in Fig. 6. In the first configuration Fig. 6(a) $\mathbf{I}_1(\kappa,\lambda)$ and $\mathbf{I}_2(\kappa,\lambda)$ are two elements vectors containing the amplitudes, in *s* and *p* polarizations, of the incident field coming from the superstrate and the substrate respectively, and $\mathbf{D}_1(\kappa,\lambda)$, $\mathbf{D}_2(\kappa,\lambda)$ stand for the diffracted field. In the second configuration Fig. 6(b), the structure is illuminated with $\mathbf{I'}_1(-\kappa,\lambda)$ and $\mathbf{I'}_2(-\kappa,\lambda)$ in such a way that $\mathbf{I'}_2(-\kappa,\lambda)$ is the symmetric of $\mathbf{I}_1(\kappa,\lambda)$ with respect to the center of symmetry C, and $\mathbf{I'}_1(-\kappa,\lambda)$) is the symmetric of $\mathbf{I}_2(\kappa,\lambda)$:

$$\begin{aligned} \mathbf{I'}_1(-\kappa,\lambda) &= \mathbf{I}_2(\kappa,\lambda) \\ \mathbf{I'}_2(-\kappa,\lambda) &= \mathbf{I}_1(\kappa,\lambda). \end{aligned} \tag{12}$$

#234212 - $15.00 USD Received 9 Feb 2015; revised 15 Apr 2015; accepted 16 Apr 2015; published 24 Apr 2015

Because the structure is symmetric with respect to C, the two configurations are physically equivalent, and we can say that the same equality is verified for the diffracted field:

$$\begin{array}{c} \mathbf{D'}_1(-\kappa,\lambda) = \mathbf{D}_2(\kappa,\lambda) \\ \mathbf{D'}_2(-\kappa,\lambda) = \mathbf{D}_1(\kappa,\lambda). \end{array} \tag{13}$$

From the definition of the scattering matrix, we write:

$$\begin{pmatrix} \mathbf{D'}_1(-\kappa,\lambda) \\ \mathbf{D'}_2(-\kappa,\lambda) \end{pmatrix} = \begin{pmatrix} \mathbf{R_1}(-\kappa,\lambda) & \mathbf{T_2}(-\kappa,\lambda) \\ \mathbf{T_1}(-\kappa,\lambda) & \mathbf{R_2}(-\kappa,\lambda) \end{pmatrix} \begin{pmatrix} \mathbf{I'}_1(-\kappa,\lambda) \\ \mathbf{I'}_2(-\kappa,\lambda) \end{pmatrix}, \tag{14}$$

and, on the other hand:

$$\begin{pmatrix} \mathbf{D}_1(\kappa,\lambda) \\ \mathbf{D}_2(\kappa,\lambda) \end{pmatrix} = \begin{pmatrix} \mathbf{R_1}(\kappa,\lambda) & \mathbf{T_2}(\kappa,\lambda) \\ \mathbf{T_1}(\kappa,\lambda) & \mathbf{R_2}(\kappa,\lambda) \end{pmatrix} \begin{pmatrix} \mathbf{I}_1(\kappa,\lambda) \\ \mathbf{I}_2(\kappa,\lambda) \end{pmatrix}. \tag{15}$$

From Eqs. (14) and (15) using Eqs. (12) and (13), we deduce that

$$\begin{array}{c} \mathbf{R_1}(-\kappa,\lambda) = \mathbf{R_2}(\kappa,\lambda) \\ \mathbf{T_1}(-\kappa,\lambda) = \mathbf{T_2}(\kappa,\lambda). \end{array} \tag{16}$$

Finally, using the reciprocity theorem Eqs. (9)–(11), it follows that

$$\begin{array}{c} \mathbf{R_1}(\kappa,\lambda) = t(\mathbf{R_2}(\kappa,\lambda)) \\ \mathbf{T_1}(\kappa,\lambda) = t(\mathbf{T_1}(\kappa,\lambda)) \\ \mathbf{T_2}(\kappa,\lambda) = t(\mathbf{T_2}(\kappa,\lambda)). \end{array} \tag{17}$$

.3. *Properties of the eigenvalues*

Let us now consider the energy transfer transmission and reflection matrices $\mathbf{T_j}^*\mathbf{T_j}$ and $\mathbf{R_j}^*\mathbf{R_j}$, with $j = 1$ or 2. We shall demonstrate that their egienvalues are unchanged when the polar angle is changed in its opposite. The two eigenvalues for each of the matrices are denoted as $l_k^{T_j^*T_j}$ and $l_k^{R_j^*R_j}$ (with $k = a$ or b), and $\mathbf{V_k^{T_j^*T_j}}$ and $\mathbf{V_k^{R_j^*R_j}}$ stand for the associated eigenvectors.

The first property comes from the energy balance. Multiplying Eq.(5) (resp. Eq.(6)) , with $\mathbf{V_k^{T_1^*T_1}}$ (resp. $\mathbf{V_k^{T_2^*T_2}}$), it is easy to show that

$$\begin{array}{c} l_k^{R_1^*R_1} = 1 - l_k^{T_1^*T_1}, \quad \text{and} \quad \mathbf{V_k^{R_1^*R_1}} = \mathbf{V_k^{T_1^*T_1}}, \\ (\text{resp.} \quad l_k^{R_2^*R_2} = 1 - l_k^{T_2^*T_2}, \quad \text{and} \quad \mathbf{V_k^{R_2^*R_2}} = \mathbf{V_k^{T_2^*T_2}}). \end{array} \tag{18}$$

The second property comes from the reciprocity theorem. Considering a given real κ, and from the definition of the eigenvalue of $\mathbf{T_1}^*(\kappa,\lambda)\mathbf{T_1}(\kappa,\lambda)$, we have $\mathbf{T_1}^*(\kappa,\lambda)\mathbf{T_1}(\kappa,\lambda)\mathbf{V_k^{T_1^*T_1}}(\kappa,\lambda) = l_k^{T_1^*T_1}(\kappa,\lambda)\mathbf{V_k^{T_1^*T_1}}(\kappa,\lambda)$. Using the relation between $\mathbf{T_1}(\kappa,\lambda)$ and $\mathbf{T_2}(-\kappa,\lambda)$ coming from the reciprocity theorem (Eq. (9)), we obtain

$$\begin{array}{c} \overline{\mathbf{T_2}}(-\kappa,\lambda)t(\mathbf{T_2}(-\kappa,\lambda))\mathbf{V_k^{T_1^*T_1}}(\kappa,\lambda) \\ = l_k^{T_1^*T_1}(\kappa,\lambda)\mathbf{V_k^{T_1^*T_1}}(\kappa,\lambda). \end{array} \tag{19}$$

Taking the complex conjugate and multiplying the two sides of Eq. (19) with $\mathbf{T_2}^*(-\kappa,\lambda)$, we obtain that

$$\begin{array}{c} \mathbf{T_2}^*(-\kappa,\lambda)\mathbf{T_2}(-\kappa,\lambda)[\mathbf{T_2}^*(-\kappa,\lambda)\overline{\mathbf{V_k^{T_1^*T_1}}}(\kappa,\lambda)] \\ = l_k^{T_1^*T_1}(\kappa,\lambda)[\mathbf{T_2}^*(-\kappa,\lambda)\overline{\mathbf{V_k^{T_1^*T_1}}}(\kappa,\lambda). \end{array} \tag{20}$$

#234212 - $15.00 USD Received 9 Feb 2015; revised 15 Apr 2015; accepted 16 Apr 2015; published 24 Apr 2015

This means that

$$\begin{aligned} l_k^{T_2^* T_2}(-\kappa,\lambda) = l_k^{T_1^* T_1}(\kappa,\lambda) \quad \text{and} \quad \mathbf{V_k^{T_2^* T_2}}(-\kappa,\lambda) \\ = \mathbf{T_2}^*(-\kappa,\lambda)\overline{\mathbf{V_k^{T_1^* T_1}}}(\kappa,\lambda). \end{aligned} \tag{21}$$

A similar demonstration using the definition of the eigenvalues of $\mathbf{R_j}^*(\kappa,\lambda)\mathbf{R_j}(\kappa,\lambda)$ (for $j=1$ or 2) and the Eqs. (10) and (11) leads to

$$\begin{aligned} l_k^{R_j^* R_j}(-\kappa,\lambda) = l_k^{R_j^* R_j}(\kappa,\lambda) \quad \text{and} \quad \mathbf{V_k^{R_j^* R_j}}(-\kappa,\lambda) \\ = \mathbf{R_j}^*(-\kappa,\lambda)\overline{\mathbf{V_k^{R_j^* R_j}}}(\kappa,\lambda), \end{aligned} \tag{22}$$

for $k=a$ and b (the two eigenvalues), and $j=1$ or 2 (the two reflectivity matrices).

Finally, applying both the energy balance and the reciprocity theorem, we obtain the following relation for the eigenvalues ($k=a$ or b):

$$l_k^{T_1^* T_1}(\kappa,\lambda) = l_k^{T_2^* T_2}(\kappa,\lambda) = l_k^{T_1^* T_1}(-\kappa,\lambda) = l_k^{T_2^* T_2}(-\kappa,\lambda), \tag{23}$$

$$l_k^{R_1^* R_1}(\kappa,\lambda) = l_k^{R_2^* R_2}(\kappa,\lambda) = l_k^{R_1^* R_1}(-\kappa,\lambda) = l_k^{R_2^* R_2}(-\kappa,\lambda). \tag{24}$$

In other words, the energy balance and the reciprocity theorem entail that the two reflectivity (resp. transmittivity) matrices for the energy have the same eigenvalues, and that these eigenvalues are symmetrical with respect to the polar angle of incidence. This last property is the vectorial analog of the property which is well known for 1D blazed gratings illuminated in classical incidence (plane of incidence perpendicular to the grating grooves). Note that the eigenvectors of the reflectivity (resp. transmittivity) matrices for the energy do change when the polar angle is changed in its opposite, which means that in case of polarization conversion, the reflected and transmitted energy are not symmetric with respect to the polar angle of incidence for any state of polarization.

.4. *Resonant behavior of the eigenvalues*

In this paragraph, we shall demonstrate that one eigenvalue of the energy transmittivity matrix $\mathbf{T_1}^*\mathbf{T_1}$ reaches 100% if the structure has a central symmetry. From now, we consider a configuration for a given real κ where only one eigenmode of the structure can be excited. This means that the equation $\det(\mathbf{S}^{-1}(\kappa,\lambda))=0$ has one complex solution $\lambda=\lambda_p(\kappa)$ where $\lambda_p(\kappa)$ stands for the dispersion relation of the eigenmode. We introduce the eigenvalues $l_a^{R_1}(\kappa,\lambda)$ and $l_b^{R_1}(\kappa,\lambda)$ and eigenvectors $\mathbf{V_a^{R_1}}(\kappa,\lambda)$ and $\mathbf{V_b^{R_1}}(\kappa,\lambda)$ of the matrix $\mathbf{R_1}$. We suppose that only one of the two eigenvalues of $\mathbf{R_1}$ shows a resonant behavior, the other remaining a slowly varying function. We have checked numerically the validity of this hypothesis for the configuration under study. Following the arguments given in [26] (end of section 4), for λ in the vicinity of $\lambda_p(\kappa)$ we write the resonant eigenvalue, say $l_a^{R_1}$, as

$$l_a^{R_1}(\kappa,\lambda) = u(\kappa,\lambda)\frac{\lambda-\lambda_z^{R_1}(\kappa)}{\lambda-\lambda_p(\kappa)}, \tag{25}$$

where $u(\kappa,\lambda)$ is a function with neither roots nor poles, and $\lambda_z^{R_1}(\kappa)$ a complex number. The unicity of the root of $l_a^{R_1}(\kappa,\lambda)$, which is due to the fact that only one mode is excited, is an important property that will be used at the end of the proof.

#234212 - $15.00 USD Received 9 Feb 2015; revised 15 Apr 2015; accepted 16 Apr 2015; published 24 Apr 2015

When $\lambda = \lambda_z^{R_1}(\kappa)$, we obtain that $\mathbf{R_1}(\kappa, \lambda_z^{R_1})\mathbf{V_a^{R_1}}(\kappa, \lambda_z^{R_1}) = 0$. Introducing this in Eq. (5), where the two sides have been multiplied with $\mathbf{V_a^{R_1}}(\kappa, \lambda_z^{R_1})$, we obtain

$$\mathbf{T_1}^*(\kappa, \overline{\lambda_z^{R_1}})\mathbf{T_1}(\kappa, \lambda_z^{R_1})\mathbf{V_a^{R_1}}(\kappa, \lambda_z^{R_1}) = \mathbf{V_a^{R_1}}(\kappa, \lambda_z^{R_1}) \tag{26}$$

which is nothing but the eigenvector equation for $\mathbf{T_1}^*\mathbf{T_1}$. This means that for $\lambda = \lambda_z^{R_1}(\kappa)$, one eigenvalue of $\mathbf{T_1}^*\mathbf{T_1}$, say $l_a^{T_1^*T_1}(\kappa, \lambda_z^{R_1})$ is equal to unity. Its eigenvector is $\mathbf{V_a^{T_1^*T_1}}(\kappa, \lambda_z^{R_1}) = \mathbf{V_a^{R_1}}(\kappa, \lambda_z^{R_1})$. In other words, and not surprisingly, for $\lambda = \lambda_z^{R_1}(\kappa)$, the maximum of transmittivity is obtained when the incident configuration leads to a zero reflected field.

We shall now prove that the symmetry of the structure with respect to a symmetry center entails the fact that $\lambda_z^{R_1}(\kappa)$ is real, meaning that the transmittivity can reach 100% for a real wavelength value. Multiplying the two sides of Eq. (8) with $\mathbf{V_a^{R_1}}(\kappa, \lambda_z^{R_1})$ and taking $\lambda = \lambda_z^{R_1}(\kappa)$ leads to

$$\mathbf{R_2}^*(\kappa, \overline{\lambda_z^{R_1}})\mathbf{T_1}(\kappa, \lambda_z^{R_1})\mathbf{V_a}(\kappa, \lambda_z^{R_1}) = 0. \tag{27}$$

Using Eq. (17), we obtain

$$\mathbf{R_1}(\kappa, \overline{\lambda_z^{R_1}})\overline{\mathbf{T_1}}(\kappa, \lambda_z^{R_1})\overline{\mathbf{V_a}}(\kappa, \lambda_z^{R_1}) = 0. \tag{28}$$

As $\mathbf{T_1}(\kappa, \lambda_z^{R_1})\mathbf{V_a}(\kappa, \lambda_z^{R_1})$ can not be null (otherwise from Eq. (26), $\mathbf{V_a}(\kappa, \lambda_z^{R_1})$ would be null), we deduce that $\overline{\mathbf{T_1}}(\kappa, \lambda_z^{R_1})\overline{\mathbf{V_a}}(\kappa, \lambda_z^{R_1})$ is the eigenvector of $\mathbf{R_1}$ associated with an eigenvalue which is null for $\lambda = \overline{\lambda_z^{R_1}}$. As $l_a^{R_1}(\kappa, \lambda)$ has only one root and $l_b^{R_1}(\kappa, \lambda)$ has no root, we conclude that $\lambda_z^{R_1}(\kappa)$ is real. Hence, we have shown that there exists one real wavelength for which one eigenvalue of the matrix $\mathbf{T_1}^*\mathbf{T_1}$ is equal to 100%.

Acknowledgments

The thesis of T. Alaridhee is funded by Iraqi government through the ministry of "Higher Education & Scientific Research". This work is partially supported by the French Center for Scientific Research (CNRS) contract "ESENCYAL" under the number ANR-13-ASTR-0019-01, by the Labex ACTION and by the Franche-Comté Unviersity computing center: "Mesocentre de calcul de Franche-Comté".

#234212 - $15.00 USD Received 9 Feb 2015; revised 15 Apr 2015; accepted 16 Apr 2015; published 24 Apr 2015